Kinematical Calibration of a Robot Manipulator for Brain Biopsy

Nuno Augusto Alves Pereira
nuno.pereira11@gmail.com

Instituto Superior Técnico, Universidade de Lisboa, Lisboa, Portugal

June 2019

Abstract – Accuracy is an important factor to guarantee because without it the work of a manipulator can not be relied on. This paper presents an algorithm to kinematically calibrate robotic manipulators based on the Denavit-Hartenberg model with a camera as a measurement device. The method applied was the linear least square identification which consisted on the use of a pseudo inverse to solve the equations and the errors were compensated numerically. The algorithm calibrates all the Denavit-Hartenberg parameters, including the offset of the joints. The simulation was completed in manipulators with two, three, six and seven joints and it presented promising results with high quality and efficiency.

Keywords: Robotics, Kinematic Calibration, Brain Biopsy, Denavit-Hartenberg, Polaris Spectra, KUKA LWR 4^+, Least Square Method.

1. INTRODUCTION

Nowadays robotics is the most feasible method to obtain good results whenever high accuracy and repeatability is required, as in the area of robotic surgery. The robotic calibration is as important as the procedure, because without it, it is not possible to guarantee accurate results.

Robotics in neurosurgery enables improvements in several aspects and execution of numerous actions, and it is also applicable to several neurosurgical applications [1,2].

There are several robots used in neurosurgery. The most common robots used are the ROSA Robot [3], the Neuromate [4], the NeuroArm [5] and the RONNA G3 [6]. They can execute procedures within accuracy between two and three millimeters [2,7].

A biopsy is a very common procedure. In a study published in 2018, which evaluates robot assisted cerebral biopsy, 18.3% of the patients had some sort of complication after the procedure. Additionally, when different methods of registration were used an accuracy of 0.3 mm was obtained [8].

Robotic calibration is a process that consists of determining the kinematic parameters that improve the accuracy of the robot and decrease the error obtained relative to the nominal parameters [9,10]. There are three levels of calibration: level one, defined as “Joint level calibration”, level three, “Dynamic model calibration”, and the focus of this work, level two, defined as “Kinematic model calibration [11]. Level two, the calibration level used in this work, can be divided into four different procedures [12]:

- Kinematic modulation
- Measurement
- Kinematic Identification
- Compensation

1.1. Kinematic Modulation

The kinematic modulation defines the kinematic model through symbolic variables that represents the robot. To achieve a good calibration the model must contain completeness, equivalence and proportionality [11].

There are several methods to represent a kinematic model. One of the most common is the Denavit-Hartenberg convention [13] that describes the relation between two consecutive frames through four coordinates. However, when two consecutives joints are parallel this method can not be used due to the singularities in the Jacobian matrix [10,11]. To overcome this obstacle, Hayati and Mirmirani modified the Denavit-Hartenberg, adding a new rotation parameter, β, that represents the misalignment of near parallel axis [14]. This model is called Hayati model or Modified Denavit-Hartenberg model. Roger W. Brockett developed the POE (Product Of Exponentials) convention that is based on the geometrical interpretation of screw theory, representing the direct kinematics as a product of exponentials matrices [15]. Zhuang et al. presented us the CPC (Complete and Parametrically Continuous) convention, named after the completeness of the model by adding two new parameters to each link and the continuity of

the parameters due to the use of a linear representation without singularities [16].

1.2. Measurements Methods

The measurements methods contemplate the devices used to this end. A measurement device should be able to obtain end-effector poses in a large work space and ideally with an accuracy that is 10 times higher than the accuracy desired for the manipulator [17]. There are several measurement methods for example tools, cameras, lasers, robotic arms, sensors, probes and others. Tools were used by some researches such as [18] and [19]. During the 1980s a specific type of cameras, theodolites, were used by [20] and [21] capable of measurements within accuracies around $0.05\ mm$. In the beginning of the century more sophisticated and cheaper methods arose, and the use of lasers together with CCD cameras became common verified in [22], [23], [24] and [25] where the camera takes measurements of a laser mounted on the manipulator in a plane. Other method, used by [26], [27], [28], [29] and [30], is a laser tracking system that consists of a mirror installed on a reference point that emits and reflects a laser beam onto a retro-reflector mounted on the end effector of the manipulator. The measurements are obtained by optical encoders and interferometers. Concerning probes, used by [31] and [32], one can be attached on the end effector and used to take measurements in a restriction plane or, by [33], a CMM (Coordinate Measurement Machine) can be used to measure the pose of the end effector. Other option to measure the end effector pose is to use a calibrated robotic arm like the ones used in [10], [34], [35] and [36].

1.3. Kinematic Identification Methods

The identification of kinematic parameters is based on the use of numerical methods [37]. To quantify the quality of the identification two parameters are used: the observability index [38] which indicates which configurations influence the error the most and the condition number of the observation matrix [39] which measures the sensitivity of the solution relative to the noise and the modeled error. The identification consists of a linear or nonlinear procedure of least square optimization [37].

Nonlinear methods that can be used are the Gauss-Newton method [32], the Lavenberg-Marquardt algorithm [10,25] and others like [33] and [30].

The linear methods require less computational time, however they have numerical problems regarding the poor Jacobian matrix condition number [37]. Some linear methods used are the Lavenberg-Marquardt in [27], neural networks in [31], extended Kalman filter in [24] and [40], minimizing a cost function in [19] and [35], pattern search algorithm in [20], Gauss elimination method in [18], the accurate forward solution developed and used by [21], amongst other methods.

1.4. Compensation Methods

Error compensation is the process of applying the identified kinematic parameters in the robot's model [17] in order to allow the robot to accomplish the desired task [12]. Besides obtaining the compensated poses the calculation of the respective parameters through inverse kinematics is one of the main obstacles encountered [17].

To overcome this obstacle there are several methods like the iterative Newton-Raphson used in [18] and [19], neural networks used in [31], [30] and [36], the error transformation compensation method referenced in [18], the accurate forward solution used in [21], the pose redefinition method use by [10] and the Euler angles formula used by [33].

1.5. Calibration Quality Study

In order to study the quality of the calibration the root mean square of the values obtained is used

$$x_{rms} = \sqrt{\frac{1}{n}(x_1^2 + x_2^2 + \cdots + x_n^2)}. \quad (1)$$

In the literature presented formerly the error values obtained by calibration were between $0.18\ mm$ and $2.85\ mm$ for position and between $0.016\ rad$ and $0.75\ rad$ for orientation. It is notable that the value obtained does not follow any type of pattern, meaning that the error value obtained is dependent on the resolution of the selected methods and not on the chosen methods themselves.

2. DEVICES

In this work the devices used are the KUKA lightweight robot 4^+ (LWR) [41] and the Polaris Spectra camera [42].

The 15 kg robot has seven degrees of freedom that makes it redundant. Each joint has a torque sensor, and with its dynamic model state control and servo controller active damping of vibrations is enabled and the robot reaches excellent kinematic performances [43]. The workspace has a volume of $1.84\ m^3$, with a documented repeatability of

$\pm 0.05\ mm$ and the robot has a recommended rated payload of seven kilograms [44].

The LWR is controlled by the KCP (Kuka Control Panel) connected to the KRC (Kuka Robot Controller). The user controls the robot using a computer that communicates with the KRC through the FRI (Fast Research Interface) and resorts to the KRL (Kuka Robot Language) which allows the control with a cycle time between one and 100 ms.

This manipulator can be used in different modes of control, for example joint specific position control where

$$\mathrm{q_{cmd}} = q_{FRI}, \tag{2}$$

joint specific impedance control where the control law is

$$\tau_{\mathrm{cmd}} = k_j(q_{FRI} - q_{msr}) + D(d_j) + \tau_{FRI} + f_{dynamics}(q, \dot{q}, \ddot{q}), \tag{3}$$

and finally cartesian impedance control where the control law is

$$\tau_{\mathrm{cmd}} = J^T(k_c(x_{FRI} - x_{msr}) + D(d_c) + F_{FRI}) + f_{dynamics}(q, \dot{q}, \ddot{q}). \tag{4}$$

The Polaris Spectra is a position and orientation tridimensional tracking optical system used in several surgical procedures.

This device has a work volume displayed in the figure below.

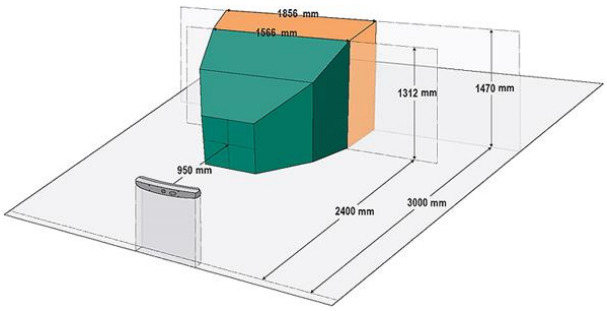

Figure 1 - Polaris Spectra work volume

It is documented that inside the work volume the device has an accuracy of $0.25\ mm\ RMS$ for the green volume and an accuracy of $0.3\ mm\ RMS$ for the orange volume.

In order to assist the measurements the Polaris resorts to markers in a form of spheres.

3. ROBOTIC KINEMATICS

A kinematic manipulator is comprised of links connected by joints that can be revolute or prismatic. One end is constrained to a base and at the other end there is an end-effector.

This structure is characterized by the number of degrees of freedom (DOF) that are normally associated with each joint. The objective of the direct kinematics is to compute the pose of the end-effector, or the position and orientation, as a function of the joint variables.

The pose of the end-effector is given by the homogeneous transformation matrix

$$T_e^b(q) = \begin{bmatrix} n_e^b(q) & s_e^b(q) & a_e^b(q) & p_e^b(q) \\ 0 & 0 & 0 & 1 \end{bmatrix}, \tag{5}$$

where p_e is the position vector and n_e, s_e, a_e are the representation of the unit vectors of a frame in the end-effector named, respectively, as normal, sliding and approach, defining the orientation of the transformation.

This matrix relates the end effector with the base frame, where n is the number of joints, by

$$T_n^0(q) = A_1^0(q_1)\mathrm{A}_2^1(\mathrm{q}_2) \dots A_n^{n-1}(q_n). \tag{6}$$

The joint parameters are defined by the Denavit-Hartenberg convention where the frame of every joint is defined following specific rules. The parameters related to each joint are defined as:

- a_i – Distance between O_i and O_i',
- d_i – Coordinate of O_i' along z_{i-1},
- α_i - z_{i-1}^z_i about x_i with positive rotation CCW,
- ν_i - x_{i-1}^x_i about z_{i-1} with positive rotation CCW.

A manipulator is called kinematically redundant when it has a number of DOF superior to the number of variables needed to accomplish a task.

The Jacobian of a manipulator is a matrix that represents the relation between linear and angular velocities of the end effector, $\dot{x}_e$ and $\dot{w}_e$, and joint velocities, $\dot{\nu}$, being function of joint variables, ν. This matrix describes the influence of each joint coordinate in the end effector relative to the base frame. The Jacobian is given by

$$J(\nu) = \begin{bmatrix} \frac{df_1}{d\nu_1} & \cdots & \frac{df_1}{d\nu_n} \\ \vdots & & \vdots \\ \frac{df_m}{d\nu_1} & \cdots & \frac{df_m}{d\nu_n} \end{bmatrix} \epsilon \mathbb{R}^{m \times n}. \tag{7}$$

Relative to the number of joint coordinates, the Jacobian matrix can be kinematically deficient, $n < 6$, square, $n = 6$, or redundant, $n > 6$, as the operational space has a maximum size of six coordinates, three from position and three from orientation.

Depending on the manipulator and the configuration of the robot a singularity may occur. A singularity represents a mechanical limit in which the mobility is reduced and makes the movement in

one or more directions impossible. In a singularity the inverse kinematics has infinite solutions. There are two types of singularities: boundary singularities that occur when the manipulator is completely stretched or retracted and internal singularities that are normally originated by the alignment of two or more axes of motion or by specific end-effector configurations.

Mathematically, in the Jacobian, a singularity is represented by null columns, internal singularities, or null rows, boundary singularities, and the rank of the matrix is less than the maximum rank of the matrix.

3.1. Kinematic Manipulators

In order to better understand the kinematics of the manipulators the kinematics of several robots using the Denavit-Hartenberg convention will be presented. The direct kinematics of each manipulator can be consulted in [45].

Two-link Planar Arm

This manipulator is a non-redundant two revolution axis robot. Due to being a planar manipulator the operational space can only have three components, two for position and one for orientation.

Three-link Planar Arm

This robot is similar to the two-link planar arm with an addition of a revolution axis. With 3 DOF this manipulator is not redundant.

Anthropomorphic Arm with Spherical Wrist

This manipulator has six rotation axis and it is not redundant because it has the number of DOF equal to the number of variables in the operational space. With the change of the value of the α_i parameter the transformation matrix is affected. In order to study the singularities of this manipulator it is decoupled in two sub structures, the anthropomorphic arm and the spherical wrist.

One singularity in the anthropomorphic arm occurs when $v_3 = 0 \vee v_3 = \pi$ and it means that the elbow is stretched or retracted, which is called elbow singularity. Other arm singularity happens when the position of the wrist is along z_0 and it is named shoulder singularity. A wrist singularity occurs when z_3 and z_5 are aligned, that is $v_5 = 0 \vee v_5 = \pi$.

DLR Manipulator

This manipulator has 7 DOF and it simulates a human arm. It is assembled by an anthropomorphic arm that simulates the shoulder, and a spherical wrist that simulates the wrist. These two parts are united by a joint simulating the elbow. This manipulator is redundant because it has more DOF than operational space variables.

To overcome the redundancy a new parameter, the swivel angle, is added, which is described by the angle α_d, along a circular arc perpendicular to the vector, y_{sw}, between the position of the wrist and the position of the shoulder. This angle is shown in the figure below.

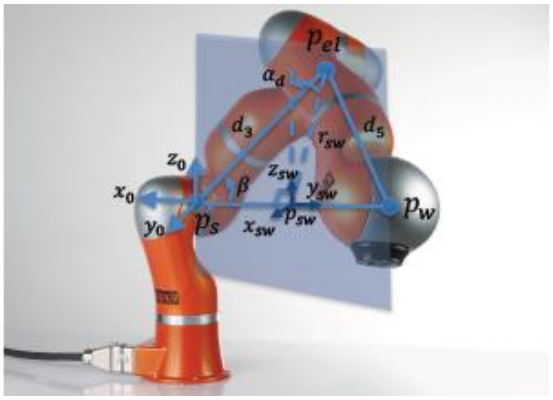

Figure 2 - Swivel Angle

Using the swivel angle it is possible to calculate the inverse kinematics [46]. This is performed through the manipulator decoupling. First the swivel reference frame is defined and then the position of the elbow is calculated, returning

$$p_{el} = R_{sw} \begin{bmatrix} r_{sw} \sin(\alpha_d) \\ p_{sw} \\ r_{sw} \cos(\alpha_d) \end{bmatrix} = \begin{bmatrix} p_{el_x} \\ p_{el_y} \\ p_{el_z} \end{bmatrix}. \quad (8)$$

To obtain v_1 and v_2 the elbow position calculated by direct kinematics is used

$$v_{2I} = Atan2\left(\sqrt{1-\cos^2(v_2)}\,, \cos(v_2)\right), \quad (9)$$

$$v_{2II} = Atan2\left(-\sqrt{1-\cos^2(v_2)}\,, \cos(v_2)\right), \quad (10)$$

$$v_{1I} = Atan2\left(-p_{el_y}, -p_{el_x}\right), \quad (11)$$

$$v_{1II} = Atan2\left(p_{el_y}, p_{el_x}\right), \quad (12)$$

with v_{2II} and v_{1II} calculated for negative $\sin(v_2)$. To acquire v_3 and v_4 the position of the wrist is calculated relative to the frame of the second joint.

$$v_{4I} = Atan2\left(\sqrt{1-\cos^2(v_4)}\,, \cos(v_4)\right), \quad (13)$$

$$v_{4II} = Atan2\left(-\sqrt{1-\cos^2(v_4)}\,, \cos(v_4)\right), \quad (14)$$

$$\nu_{3I} = Atan2\left({}^{2}p_{w_y}, {}^{2}p_{w_x}\right), \quad (15)$$

$$\nu_{3II} = Atan2\left(-{}^{2}p_{w_y}, -{}^{2}p_{w_x}\right), \quad (16)$$

with ν_{4II} and ν_{3II} calculated for negative $\sin(\nu_4)$. For the last three joints, ν_5, ν_6 and ν_7, the rotation matrix between the frame of the seventh joint and the frame of the fourth joint,

$$\nu_{5I} = Atan2(-r_{23}, -r_{13}), \quad (17)$$

$$\nu_{6I} = Atan2\left(\sqrt{r_{31}^2 + r_{32}^2}, r_{33}\right), \quad (18)$$

$$\nu_{7I} = Atan2(-r_{32}, -r_{31}), \quad (19)$$

and for a negative $\sin(\nu_6)$

$$\nu_{5II} = Atan2(r_{23}, r_{13}), \quad (20)$$

$$\nu_{6II} = Atan2\left(-\sqrt{r_{31}^2 + r_{32}^2}, r_{33}\right), \quad (21)$$

$$\nu_{7II} = Atan2(r_{32}, -r_{31}), \quad (22)$$

Related to the redundancy, this manipulator can have several configurations for the same end-effector pose. This set of configurations is called the null space.

The redundancy can be verified by the calculation of the rank of the matrix that will be less than the number of DOF. If a singularity occurs, the rank of the matrix will be even smaller, which implies a kinematic deficiency and the pose of the end-effector could not be completely defined.

For this manipulator there are several possible singularities. One happens when the position of the wrist is aligned with the shoulder along z_0. Other singularity is verified when the swivel arc is zero and it means that the position of the shoulder, elbow and wrist is aligned. When the position of the elbow is aligned with the should along z_0 and when $\nu_6 = 0 \vee \nu_6 = \pi$, z_4 and z_6 are aligned and there is an internal singularity that can be overcome by a different swivel angle.

4. Kinematic Calibration

Kinematic calibration is the procedure to estimate the Denavit-Hartenberg parameters that increase the accuracy of the manipulator.

The direct kinematics is described with

$$x_e = f(a, \alpha, d, \nu), \quad (23)$$

where x_e is the end-effector posture described by its position and orientation. f is the relation between the operation space and the Denavit-Hartenberg parameters.

$$a = \begin{bmatrix} a_1 \\ . \\ . \\ . \\ a_n \end{bmatrix}, \quad \alpha = \begin{bmatrix} \alpha_1 \\ . \\ . \\ . \\ \alpha_n \end{bmatrix}, \quad d = \begin{bmatrix} d_1 \\ . \\ . \\ . \\ d_n \end{bmatrix}, \quad \nu = \begin{bmatrix} \nu_1 \\ . \\ . \\ . \\ \nu_n \end{bmatrix}. \quad (24)$$

In the calibration there is nominal data, index n, determined by the robot controller, and the measured data, index m, defined by the measurement device. The posture accuracy, Δx, is given by the difference between the measured posture, x_m, and the nominal one, x_n.

$$\Delta x = x_m - x_n. \quad (25)$$

Assuming small variations the posture accuracy is given by

$$\Delta x = \frac{\delta f}{\delta a}\Delta a + \frac{\delta f}{\delta \alpha}\Delta \alpha + \frac{\delta f}{\delta d}\Delta d + \frac{\delta f}{\delta \nu}\Delta \nu. \quad (26)$$

In the previous equation, $\Delta a, \Delta \alpha, \Delta d, \Delta \nu$ are the difference between the "perfect" and nominal Denavit-Hartenberg parameters. $\frac{\delta f}{\delta a}, \frac{\delta f}{\delta \alpha}, \frac{\delta f}{\delta d}, \frac{\delta f}{\delta \nu}$, are the partial Jacobians estimated in nominal conditions.

The parameters of the manipulator are grouped in $\zeta = [a\ d\ \nu\ \alpha]$ with dimension $[4n \times 1]$, and the parameter variation, $\Delta\zeta$, is given by

$$\Delta\zeta = \zeta_m - \zeta_n. \quad (27)$$

The partial Jacobian, or partial derivatives, are grouped in a kinematic calibration matrix, or regressor matrix with dimension $[m \times 4n]$.

Combining the previous concepts, the equation (26) is rewritten as

$$\Delta x = \Phi(\zeta_n)\Delta\zeta, \quad (28)$$

and it is called the calibration equation. This equation is used to calculate $\Delta\zeta$ in order to obtain the parameters, ζ', that present the best accuracy through the nominal parameters.

In (28) an equation system is presented with m equations and $4n$ variables, where n is the number of variables and $m < 4n$. To solve the system a number of, l, end-effector posture is needed to have at least $4n$ equations. Relative to the measured postures one obtains

$$\Delta\bar{x} = \begin{bmatrix} \Delta x_1 \\ . \\ . \\ . \\ \Delta x_l \end{bmatrix}, \quad (29)$$

and

$$\bar{\Phi} = \begin{bmatrix} \Phi_1 \\ . \\ . \\ . \\ \phi_l \end{bmatrix}. \quad (30)$$

The matrixes Φ_i have the same nominal geometric parameters with different joint values dependent on the posture i.

To avoid a bad condition number of Φ, l should be chose in a way that $lm \gg 4n$. To solve (28) a least square method is used,

$$\Delta\zeta = (\bar{\Phi}^T\bar{\Phi})^{-1}\bar{\Phi}^T\Delta\bar{x}, \quad (31)$$

where $(\bar{\Phi}^T\bar{\Phi})^{-1}\bar{\Phi}^T$ ($\bar{\Phi}^{\#}$) is the pseudo-inverse of $\bar{\Phi}$.

With (31) solved it is possible to get an estimation of the parameters that improve the accuracy

$$\zeta' = \zeta_n + \Delta\zeta. \quad (32)$$

As the process is nonlinear it should be iterated until $\Delta\zeta$ converge to an established threshold. In each iteration, ζ' is used to update the values of $\bar{\Phi}$ and $\Delta\bar{x}$ used for the next iteration.

4.1. Regressor Matrix

The regressor matrix, Φ, briefly described before, is a $[m \times 4n]$ matrix, where each row is the partial derivative with respect to the coordinate m of the direct kinematics relative to a parameter n. Each joint is represented by 4 parameters, and as such, Φ, has $4n$ columns.

In this algorithm the row size of the matrix Φ is related with the number of points chosen to the trajectory. Therefore, each point of the trajectory results in a different regressor matrix, and, correspondently, the matrix Φ has $6l$ rows.

Regarding the condition number of the matrix Φ, if it is less than the number of columns, this means that there are dependent columns that need to be removed and couple the respective parameters. If the column y is dependent on the column x the coupling factor between them is

$$\frac{\zeta_y}{\zeta_x}. \quad (33)$$

4.2. Trajectory Planning

To avoid singularities and loss of rank of the matrix Φ trajectory planning is implemented.

For this case a figurative brain with a volume between $948.4\ cm^3$ and $1456.8\ cm^3$ [47] and a circumference between $55.2\ cm$ and $57.2\ cm$ [48] was used to represent the operational space of the algorithm.

For the manipulator with 2, 3 and 6 joints the nominal parameters are defined with variables between zero and $\frac{\pi}{2}$ to simulate the inverse kinematics.

For the redundant robot the center of the operational space is defined relative to the base with $x = 0.3\ m, y = 0.3\ m$ e $z = 0.2\ m$. A random volume of l points is defined, in which the inverse kinematic is applied assuming a specific swivel angle to obtain the joint variables.

4.3. Algorithm

The kinematic calibration described in 4 can be described through a step algorithm.

1. $\Delta\bar{x} = \bar{\Phi}\Delta\zeta$
2. $\Delta\zeta = \bar{\Phi}^{\#}\Delta\bar{x}$ → linear identification method
3. $\zeta' = \zeta_n + \Delta\zeta$ → new set of Denavit-Hartenberg parameters which includes the offset of ν
4. $\Delta\bar{x}' = \bar{\Phi}'\Delta\zeta$ → $\Delta\bar{x}'$ e $\bar{\Phi}'$ updated with the new ζ'
5. Repeat step 2, 3, 4 until $\Delta\zeta$ respects the established threshold.

5. RESULTS

The algorithm developed was tested in the manipulators described in the chapter 3.1 in order to study the efficiency of the algorithm with different complexity manipulators.

In this study the results compared are the mean of the rooted mean square error after the calibration in mm for the position, in degrees (°) for the orientation and in seconds (s) for the computation time. The algorithm was tested for trajectories with different number of points related to a factor Nm, that multiplied with the number of joint, j, and results in the number of points of the trajectory.

All nominal and ideal parameters are simulated.

5.1. Simulation Setup

To the planar manipulators the trajectory was simulated with joint values between $[0,90]$°. When the end-effector pose is not being influenced by the parameter "d" they correspond to dependent columns and decrease the rank of the regressor matrix causing the need to remove them and copulate the respective parameters.

After the application of the calibration algorithm the convergence was verified with mean values in the order of $4 \times 10^{-14} mm$ and $5 \times 10^{-13} \circ$ for position and orientation of the two joint planar arm and $1 \times 10^{-14} mm$ and $4 \times 10^{-13} \circ$ for position and orientation of the three joint planar arm with mean time smaller than $1.5 s$ for all different Nm.

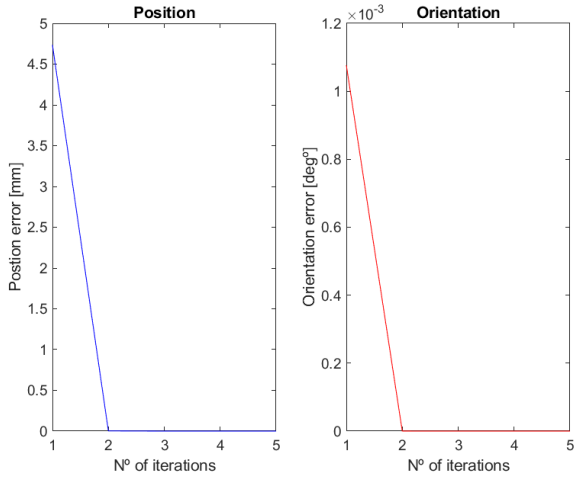

Figure 3 - Pose error evolution for two joints planar arm

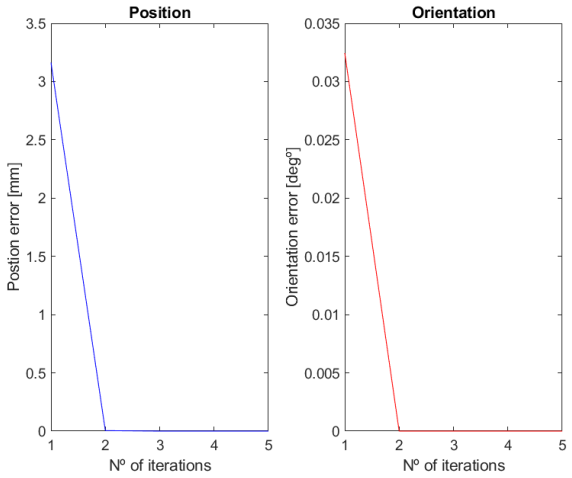

Figure 4 - Pose error evolution for three joints planar arm

The convergency is shown in the Figure 3 for two link planar arm and Figure 4 for three link planar arm above.

The six joints manipulator was simulated with joint comprehended between $[30,60]°$.

When analyzing the effect of the calibration a mean error obtained was $1 \times 10^{-13} mm$ and $2 \times 10^{-16} \circ$ for position and orientation for all different Nm. Regarding the computation times, as expected, it was noticed that with the higher number of points in the trajectory the longer was the computation time which was between $17 s$ and $92 s$. Comparing with the planar arms it was verified that, as expected, it took more iterations to converge, from two iterations to around 10 iterations as verified in the figure above.

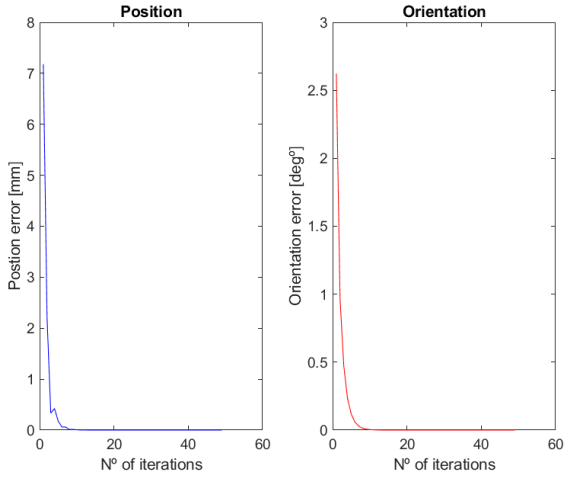

Figure 5 - Pose error evolution for six joints planar arm

As regards the seven joints manipulator instead of defining the joints angle values a cloud of points was established and the inverse kinematics to obtain the joint angles was applied.

In the same way as the other manipulators the factor Nm did not influence the error, only the computation time. As visible in the figure above the convergency was obtained efficiently.

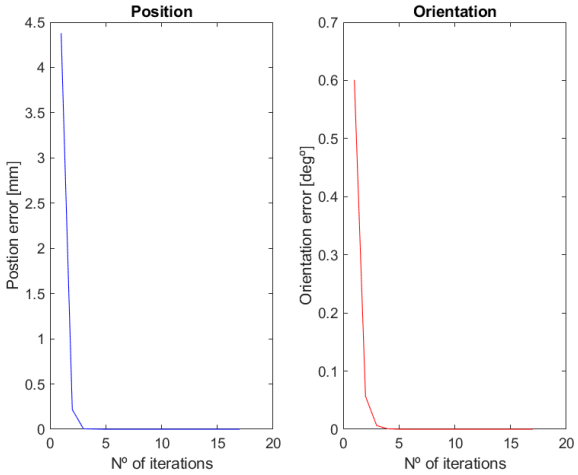

Figure 6 - Pose error evolution for seven joints planar arm

Due to the prior trajectory planning with the removal of points which results in singularities it is verified that the algorithm took less iterations to converge relatively to the six joints manipulators. It is also notable that the times of the simulations are smaller compared to the same manipulator, for each factor Nm as verified in error and the values of the times of the table above.

Table 1 - Pose Error for seven joints arm

Nm	$\left(\bar{e}_p \pm \sigma_{e_p}\right)$	$\left(\bar{e}_\phi \pm \sigma_{e_\phi}\right)$	t
400	8.35 ± 1.34	2.18 ± 0.39	8.74
600	7.84 ± 0.81	2.06 ± 0.23	18.28
800	8.18 ± 0.97	2.15 ± 0.33	35.11
1000	8.40 ± 0.81	2.24 ± 0.22	60.35

The errors exposed have an order of 10^{-4} for position and 10^{-6} for orientation in the figure above and they were obtained with a swivel angle of $\approx 0°$. It was noted that when the swivel angle was increased the error increased in order of one decimal point to around $2 \times 10^{-3} mm$ for position and remained similar to orientation.

It was seen that with a factor Nm equal 500 varying the swivel angle the errors stayed similar but the computation times slightly increased as verified in Table 2.

Table 2 - Computation time with different swivel angles

α_d	t	α_d	t
$\approx 0°$	13.25	$30°$	14.81
$15°$	13.06	$45°$	15.43
$18°$	13.19	$60°$	17.34
$22.5°$	13.59	$90°$	20.97

Regardless of the varied parameters this algorithm presented quality results and reduced computation times.

6. CONCLUSION

This work presented a way to calibrate robotic manipulators used in any area of study. The calibration objective is to present high accuracy of the manipulator after applied. The algorithm was applied using a linear identification method and was simulated in the computer through MATLAB. All the necessary values were simulated as close as in reality, the Denavit-Hartenberg parameters and the pose obtained by the Polaris Spectra Camera.

For this simulation promising calibration values were obtained relatively to the existing literature about the subject. As such in the future the algorithm should be adapted and tested in real conditions in order to test the quality obtained in the simulations.

REFERENCES

[1] Louw, D. F., Fielding, T., McBeth, P. B., Gregoris, D., Newhook, P., and Sutherland, G. R., 2004, “Surgical Robotics: A Review and Neurosurgical Prototype Development,” Neurosurgery, **54**(3), pp. 525–537.

[2] Zamorano, L., Li, Q., Jain, S., and Kaur, G., 2004, “Robotics in Neurosurgery:State of the Art and Future Technological Challenges,” Int. J. Med. Robot. Comput. Assist. Surg., **01**(01), p. 7.

[3] Vadera, S., Chan, A., Lo, T., Gill, A., Morenkova, A., Phielipp, N. M., Hermanowicz, N., and Hsu, F. P. K., 2017, “Frameless Stereotactic Robot-Assisted Subthalamic Nucleus Deep Brain Stimulation: Case Report,” World Neurosurg.

[4] Benabid, A. L., Cinquin, P., Lavalle, S., Le Bas, J. F., Demongeot, J., and De Rougemon, J., 1987, “Computer-Driven Robot for Stereotactic Surgery Connected to Ct Scan and Magnetic Resonance Imaging: Technological Design Andpreliminary Results,” Stereotact. Funct. Neurosurg.

[5] Louw, D. F., Fielding, T., McBeth, P. B., Gregoris, D., Newhook, P., and Sutherland, G. R., 2004, “Surgical Robotics: A Review and Neurosurgical Prototype Development,” Neurosurgery, **54**(3), pp. 525–537.

[6] Svaco, M., Sekoranja, B., Suligoj, F., Vidakovi, J., Jerbi, B., and Chudy, D., 2017, “A Novel Robotic Neuronavigation System: RONNA G3,” Stroj. Vestnik/Journal Mech. Eng., **63**(12), pp. 725–735.

[7] Dlaka, D., Švaco, M., Chudy, D., Jerbić, B., Šekoranja, B., Šuligoj, F., Vidaković, J., Almahariq, F., and Romić, D., 2018, “Brain Biopsy Performed with the RONNA G3 System: A Case Study on Using a Novel Robotic Navigation Device for Stereotactic Neurosurgery,” Int. J. Med. Robot. Comput. Assist. Surg., **14**(1), pp. 1–7.

[8] Terrier, L., Gilard, V., Marguet, F., and Fontanilles, M., 2019, “Stereotactic Brain Biopsy : Evaluation of Robot-Assisted Procedure in 60 Patients.”

[9] Ziegert, J., and Datseris, P., 1988, “Basic Considerations for Robot Calibration,” Proceedings. 1988 IEEE Int. Conf. Robot. Autom., pp. 932–938.

[10] Ginani, L. S., and Motta, J. M. S. T., 2011, “Theoretical and Practical Aspects of Robot Calibration with Experimental Verification,” J. Brazilian Soc. Mech. Sci. Eng., **33**(1), pp. 15–21.

[11] Everett, L., Driels, M., and Mooring, B., 1987, “Kinematic Modelling for Robot Calibration,” Proceedings. 1987 IEEE Int. Conf. Robot. Autom., **4**, pp. 183–189.

[12] Bai, Y., Zhuang, H., and Roth, Z. S., 2003, “Experiment Study of PUMA Robot Calibration Using a Laser Tracking System,” SMCia 2003 - Proc. 2003 IEEE Int. Work. Soft Comput. Ind. Appl., pp. 139–144.

[13] Denavit, J., and Hartenberg, R. S., 1955, “A Kinematic Notation for Lower-Pair Mechanisms Based on Metrics,” Trans. ASME. J. Appl. Mech.

[14] Hayati, S., and Mirmirani, M., 1985, “Improving the Absolute Positioning Accuracy of Robot Manipulators,” J. Robot. Syst., **2**(4), pp. 397–413.

[15] R.W., B., 1984, “Robotic Manipulators and the Product of Exponentials Formula,” *Mathematical Theory of Networks and Systems*, F. P.A., ed., pp. 120–129.

[16] Zhuang, H., Raton, B., Hamano, F., and Beach, L., 1990, “A Complete and Parametrically Continuous .Pdf,” pp. 92–97.

[17] Karan, B., and Vukobratović, M., 1994, “Calibration and Accuracy of Manipulation Robot Models-An Overview,” Mech. Mach. Theory, **29**(3), pp. 479–500.

[18] Veitschegger, W., and Chi-haur Wu, 1987, “A Method for Calibrating and Compensating Robot Kinematic Errors,” Proceedings. 1987 IEEE Int. Conf. Robot. Autom., **4**(3), pp. 39–44.

[19] Hanus, R., Rossignol, E., and Becquet, M., 1991, “Kinematic Calibration and Geometrical Parameter Identification for Robots,” IEEE Trans. Robot. Autom., **7**(6), pp. 721–732.

[20] Whitney, D. E., Lozinski, C. A., and Rourke, J. M., 1986, “Industrial Robot Forward Calibration Method and Results,” J. Dyn. Syst. Meas. Control, **108**(1), pp. 1–8.

[21] Judd, R. P., and Knasinski, A. B., 1990, “A Technique to Calibrate Industrial Robots with Experimental Verification,” IEEE Trans. Robot. Autom., **6**(1), pp. 20–30.

[22] Sun Lei, Liu Jingtai, Sun Weiwei, Wu Shuihua, H. X., 2004, “Geometry-Based Robot Calibration Method,” (April), pp. 1907–1912.

[23] Wang, W., Li, A., and Wu, D., 2009, “Robot Calibration by Observing a Virtual Fixed Point,” 2009 IEEE Int. Conf. Robot. Biomimetics, ROBIO 2009, pp. 1351–1355.

[24] Park, I. W., Lee, B. J., Cho, S. H., Hong, Y. D., and Kim, J. H., 2012, “Laser-Based Kinematic Calibration of Robot Manipulator Using Differential Kinematics,” IEEE/ASME Trans. Mechatronics, **17**(6), pp. 1059–1067.

[25] Hu, J. S., Wang, J. J., and Chang, Y. J., 2012, “Kinematic Calibration of Manipulator Using Single Laser Pointer,” IEEE Int. Conf. Intell. Robot. Syst., pp. 426–430.

[26] Newman, W. S., and Osborn, D. W., 1993, “A New Method for Kinematic Parameter.Pdf,” pp. 160–165.

[27] Chen, G., Wang, H., and Lin, Z., 2014, “Determination of the Identifiable Parameters in Robot Calibration Based on the POE Formula,” IEEE Trans. Robot., **30**(5), pp. 1066–1077.

[28] Li, C., Wu, Y., Lowe, H., and Li, Z., 2016, “POE-Based Robot Kinematic Calibration Using Axis Configuration Space and the Adjoint Error Model,” IEEE Trans. Robot., **32**(5), pp. 1264–1279.

[29] Martinelli, A., Tomatis, N., Tapus, A., and Siegwart, R., 2003, “Simultaneous Localization and Odometry Calibration for Mobile Robot,” Intell. Robot. Syst. 2003. (IROS 2003). Proceedings. 2003 IEEE/RSJ Int. Conf., **2**(October), pp. 1499–1504 vol.2.

[30] Aoyagi, S., Kohama, A., Nakata, Y., Hayano, Y., and Suzuki, M., 2010, “Improvement of Robot Accuracy by Calibrating Kinematic Model Using a Laser Tracking System - Compensation of Non-Geometric Errors Using Neural Networks and Selection of Optimal Measuring Points Using Genetic Algorithm-,” IEEE/RSJ 2010 Int. Conf. Intell. Robot. Syst. IROS 2010 - Conf. Proc., pp. 5660–5665.

[31] Zhong, X. L., and Lewis, J. M., 1995, “New Method for Autonomous Robot Calibration,” Proc. - IEEE Int. Conf. Robot. Autom., **2**(Figure 2), pp. 1790–1795.

[32] Ikits, M., and Hollerbach, J. M., 1997, “Kinematic Calibration Using a Plane Constraint,” Proc. Int. Conf. Robot. Autom., **4**(April), pp. 3191–3196.

[33] Katsiaris, P. T., Adams, G., Pollard, S., and Simske, S. J., 2017, “A Kinematic Calibration Technique for Robotic Manipulators with Multiple Degrees of Freedom,” IEEE/ASME Int. Conf. Adv. Intell. Mechatronics, AIM, pp. 358–363.

[34] Mustafa, S. K., Yang, G., Yeo, S. H., and Lin,

W., 2008, “Kinematic Calibration of a 7-DOF Self-Calibrated Modular Cable-Driven Robotic Arm,” Proc. - IEEE Int. Conf. Robot. Autom., pp. 1288–1293.
[35] Wu, L., Yang, X., Chen, K., and Ren, H., 2015, “A Minimal POE-Based Model for Robotic Kinematic Calibration with Only Position Measurements,” IEEE Trans. Autom. Sci. Eng., **12**(2), pp. 758–763.
[36] Liu, J., Zhang, Y., and Li, Z., 2007, “Improving the Positioning Accuracy of a Neurosurgical Robot System,” IEEE/ASME Trans. Mechatronics, **12**(5), pp. 527–533.
[37] Elatta, A, Y., Gen, L, P., Zhi, F, L., Daoyuan, Y., and Fei, L., 2004, “An Overview of Robot Calibration.Pdf,” Inf. Technol. J., pp. 74–78.
[38] Borm, J.-H., and Menq, C.-H., 1989, “Experimental Study of Observability of Parameter Errors in Robot Calibration,” Proceedings, 1989 Int. Conf. Robot. Autom., pp. 587–592.
[39] Khalil, W., Gautier, M., and Enguehard, C., 1991, “Identifiable Parameters and Optimum Configurations for Robots Calibration,” Robotica, **9**(1), pp. 63–70.
[40] Du, G., and Zhang, P., 2014, “Online Serial Manipulator Calibration Based on Multisensory Process via Extended Kalman and Particle Filters,” IEEE Trans. Ind. Electron., **61**(12), pp. 6852–6859.
[41] Schreiber, G., Stemmer, A., and Bischoff, R., 2010, “The Fast Research Interface for the Kuka Lightweight Robot,” IEEE Work. Innov. Robot Control Archit. Demanding Appl. How to Modify Enhanc. Commer. Control. (ICRA 2010), pp. 15–21.
[42] “Medical Polaris Spectra and Vicra” [Online]. Available: https://www.ndigital.com/medical/products/polaris-family/. [Accessed: 20-May-2019].
[43] Bischoff, R., Kurth, J., Schreiber, G., Koeppe, R., Albu-Schaeffer, A., Beyer, A., Eiberger, O., Haddadin, S., Stemmer, A., Grunwald, G., and Hirzinger, G., 2010, “The KUKA-DLR Lightweight Robot Arm - a New Reference Platform for Robotics Research and Manufacturing,” 41st Int. Symp. Robot. 6th Ger. Conf. Robot., (June 2014), pp. 1–8.
[44] KUKA Roboter, G., 2011, “Lightweight Robot 4 +.”
[45] Siciliano, B., Sciavicco, L., Villani, L., and Oriolo, G., 2009, *Robotics: Modelling, Planning and Control*, Springer London, London.
[46] Filipe, H., and Franco, D., 2016, “Redundancy Resolution and Inertia Reduction in KUKA LWR Robot.”
[47] Allen, J. S., Damasio, H., and Grabowski, T. J., 2002, “Normal Neuroanatomical Variation in the Human Brain: An MRI-Volumetric Study,” Am. J. Phys. Anthropol.
[48] Bushby, K. M. D., Cole, T., Matthews, J. N. S., and Goodship, J. A., 1992, “Centiles for Adult Head Circumference,” Arch. Dis. Child.